Optical measurement of mGluR1 conformational changes reveals fast activation, slow deactivation, and sensitization

Païkan Marcaggi[a,b,1], Hiroki Mutoh[b], Dimitar Dimitrov[b], Marco Beato[a], and Thomas Knöpfel[b]

[a]Department of Neuroscience, Physiology, and Pharmacology, University College London, Gower Street, London WC1E 6BT, United Kingdom; and [b]Laboratory for Neuronal Circuit Dynamics, Brain Science Institute, RIKEN, Saitama 351-0198, Japan

Edited by David E. Clapham, Harvard Medical School, Boston, MA, and approved May 18, 2009 (received for review February 6, 2009)

Metabotropic glutamate receptor (mGluR) activation has been extensively studied under steady-state conditions. However, at central synapses, mGluRs are exposed to brief submillisecond glutamate transients and may not reach steady-state. The lack of information on the kinetics of mGluR activation impairs accurate predictions of their operation during synaptic transmission. Here, we report experiments designed to investigate mGluR kinetics in real-time. We inserted either CFP or YFP into the second intracellular loop of mGluR1β. When these constructs were coexpressed in PC12 cells, glutamate application induced a conformational change that could be monitored, using fluorescence resonance energy transfer (FRET), with an EC_{50} of 7.5 μM. The FRET response was mimicked by the agonist DHPG, abolished by the competitive antagonist MCPG, and partially inhibited by mGluR1-selective allosteric modulators. These results suggest that the FRET response reports active conformations of mGluR1 dimers. The solution exchange at the cell membrane was optimized for voltage-clamped cells by recording the current induced by co-application of 30 mM potassium. When glutamate was applied at increasing concentrations up to 2 mM, the activation time course decreased to a minimum of approximately 10 ms, whereas the deactivation time course remained constant (~50 ms). During long-lasting applications, no desensitization was observed. In contrast, we observed a robust sensitization of the FRET response that developed over approximately 400 ms. Activation, deactivation, and sensitization time courses and amplitudes were used to derive a kinetic scheme and rate constants, from which we inferred the EC_{50} and frequency dependence of mGluR1 activation under non-steady-state conditions, as occurs during synaptic transmission.

G-protein coupled receptor | GPCR | imaging | glutamate sensor | dimer

The amino acid L-glutamate, the main neurotransmitter in the CNS, is referred to as a fast neurotransmitter because it mediates fast excitatory neurotransmission by activating ionotropic glutamate receptors (i.e., NMDA, AMPA, and kainate receptors). It also targets metabotropic glutamate receptors (mGluRs, 8 types) that belong to the class C G protein-coupled receptor (GPCR) subfamily. As opposed to ionotropic glutamate receptors, mGluRs mediate slower effects of glutamate, downstream of G protein activation (1). In addition, mGluRs have often been considered to play a role as extrasynaptic receptors because they are not located within the synaptic cleft (2), and their affinity for glutamate may be high enough (3) to detect glutamate concentration in extrasynaptic locations. Their extrasynaptic localization appears consistent with the slow effects of their activation because glutamate transients are expected to be less sudden at extra- and perisynaptic sites than opposite to the release site. However, even at extrasynaptic locations, glutamate transients evoked by synaptically released glutamate occur within milliseconds, as shown by recording of glutamate transporter-mediated currents in glial cells that wrap around synapses (4, 5). It is therefore necessary to determine the real-time kinetics of mGluR activation to understand how they get activated during synaptic transmission, in physiological conditions.

Traditionally, monitoring activation of native GPCRs is done by detection of events downstream in a cascade initiated by G-protein activation. These events are often delayed (by hundreds of milliseconds) and do not reflect the real-time activation of the receptor, that is, the conformational change from an inactive to an active state. Recently, activation of some class A (rhodopsin-like) GPCRs has been monitored in real-time by using a fluorescence resonance energy transfer (FRET)-based approach (6). The FRET responses observed upon agonist binding were well described by mono-exponential fits whose time constants were faster than previously expected: approximately 40 ms for the α_{2A}-adrenergic receptor (7), 70 ms for the A_{2A}-adenosine receptor (8), and 60 ms for the β_1-adrenergic receptor (9), although not as fast as for light receptor rhodopsin (10) and ligand-gated ion channels (11).

A distinctive feature of class C GPCRs is a very large extracellular domain (12), comprising a noteworthy Venus Flytrap module (VFTM), a bilobate structure in the cleft of which the agonist binds and induces its closure (13, 14). Compared with other classes, the overall conformational change leading to activation of class C GPCRs appears more complex since it is preceded by the closure of the VFTM (12), an additional step that may delay activation. However, since ionotropic glutamate receptors whose extracellular ligand-binding domain is also homologous to the VFTM activate within tens of microseconds following binding of glutamate (15), fast kinetics may be expected for class C GPCRs despite their large extracellular structure.

To investigate these kinetics, we used a FRET approach similar to that which led to the determination of the fast activation rate of members of the class A GPCRs (6–9). Type 1 mGluRs function in synaptic transmission has attracted particular interest (16) since they were shown to mediate slow synaptic excitatory currents (17) and long-term plasticity (18). Here, we report the kinetics of mGluR1β conformational changes. We show unexpected fast activation (~10 ms), slow deactivation (~50 ms), and sensitization. We derive from these results a kinetic scheme for mGluR1 activation.

Results

FRET Monitoring of Conformational Changes of mGluR1β Dimers. In our FRET approach, we took advantage of the well characterized constitutive dimerization of class C GPCRs (12, 14, 19). Structural studies have predicted that activation is produced by a reorientation of the VFTM, bringing closer together the bundles of the 7 transmembrane helix (heptahelical domains, HD) of each subunit

Author contributions: P.M. and T.K. designed research; P.M., H.M., D.D., and M.B. performed research; P.M. and M.B. analyzed data; and P.M., M.B., and T.K. wrote the paper.

The authors declare no conflict of interest.

This article is a PNAS Direct Submission.

Freely available online through the PNAS open access option.

[1]To whom correspondence should be addressed. E-mail: p.marcaggi@ucl.ac.uk.

This article contains supporting information online at www.pnas.org/cgi/content/full/0901290106/DCSupplemental.

www.pnas.org/cgi/doi/10.1073/pnas.0901290106

(12, 14, 20). According to these predictions, we inserted cyan or yellow fluorescent proteins (CFP or YFP) into the second intracellular loop of mGluR1β so that the FRET measured upon CFP excitation increases when the HDs get rearranged in the active conformations of the dimer (Fig. 1*A* and *B*). When coexpressed in PC12 cells, fluorescence imaging showed that mGluR1β-CFP and mGluR1β-YFP were localized largely at the cytoplasmic membrane (Fig. 1*C* and *D* and Fig. S1*A*) unlike the similar constructs of mGluR1α previously reported (21, 22). The fluorescence emission spectrum of co-expressing cells showed a prominent YFP emission when CFP was excited at 444 nm. Calculation of apparent FRET efficiency from fluorescence emission spectra confirmed that a large portion of this YFP emission observed with excitation in the CFP absorption band represents FRET (Fig. S1), confirming that a significant fraction mGluR1s dimerize. Superfusion of glutamate induced a reversible increase in the FRET signal (Fig. S2) as expected (Fig. 1*B*).

The FRET Response as an Index of mGluR1 Active States. The FRET response could be more precisely analyzed when glutamate was applied for a brief duration by a fast solution exchange system (Fig. 1*E* compared with Fig. S2). The averaged FRET response to 200 μM glutamate was 0.62 $\pm$ 0.06% ($\Delta R/R_0$, n = 18). The group I mGluR agonist DHPG induced a FRET response 73.9 $\pm$ 3.2% weaker than the response to glutamate (n = 5; Fig. 1*E* and *F*) as expected from the effect of DHPG in conventional mGluR1 activation assays (23). Neither the responses to 200 μM (n = 3) or 15 μM (n = 3) glutamate were affected by 1 μM JNJ 16259685 (P = 0.85 and P = 0.41 respectively; Fig. 1*G* and *H*), a potent mGluR1 non-competitive antagonist. The less potent and more commonly used mGluR1 non-competitive antagonist CPCCOEt significantly inhibited the response to glutamate, but only by 23 $\pm$ 3% (n = 6, P = 0.001; Fig. 1*G*). The non-competitive antagonist Bay 36–7620 had a stronger inhibitory effect (51 $\pm$ 4%, n = 5, P = 0.0003; Fig. 1*H*). However, contrary to what may have been expected from its reported inverse agonist effect (24), it had no significant effect on its own (n = 7, P = 0.43). The weak inhibitions observed with allosteric inhibitors JNJ 16259685, CPCCOEt, and Bay 36–7620 (whose sites and mechanisms of action are poorly understood) suggest that part of their effects occur downstream of the monitored conformational change induced by glutamate binding (for example, they may interfere with the coupling to G proteins). In contrast, the response to 15 μM glutamate was abolished by the mGluR competitive antagonist MCPG (1 mM) (96 $\pm$ 4% inhibition, n = 14, P = 10^{-10}, Fig. 1*H*). The EC_{50} of the activation by glutamate and DHPG was 7.5 μM (Fig. 1*I*). These data show that the properties of the FRET response induced by glutamate binding are similar to the activation properties of native mGluR1 monitored by the conventional indirect approaches, supporting the use of the FRET response to detect states equivalent to the active states of native mGluR1 resulting from glutamate binding.

Undetectable Activation Delay. The downstream effects of synaptic activation of native mGluR1 are observed with a delay of 50–200 ms (17, 25, 26). It is unclear whether part of this delay occurs at the level of agonist induced rearrangements of the mGluR1 dimeric assembly. To examine this issue, we performed fast glutamate application on voltage-clamped cells and monitored the solution exchange at the cell membrane by recording the current produced by co-application of 30 mM K^+. Fig. S3 shows an averaging of recordings from 27 cells to which 200 μM glutamate and 30 mM K^+ were co-applied. The onsets of the K^+ current and the fluorescence change appear to coincide. We conclude that the delay between glutamate binding and the intracellular conformational change monitored as FRET response is below our detection limit (<2 ms) and does not account for the delayed downstream effects of activation of native mGluR1.

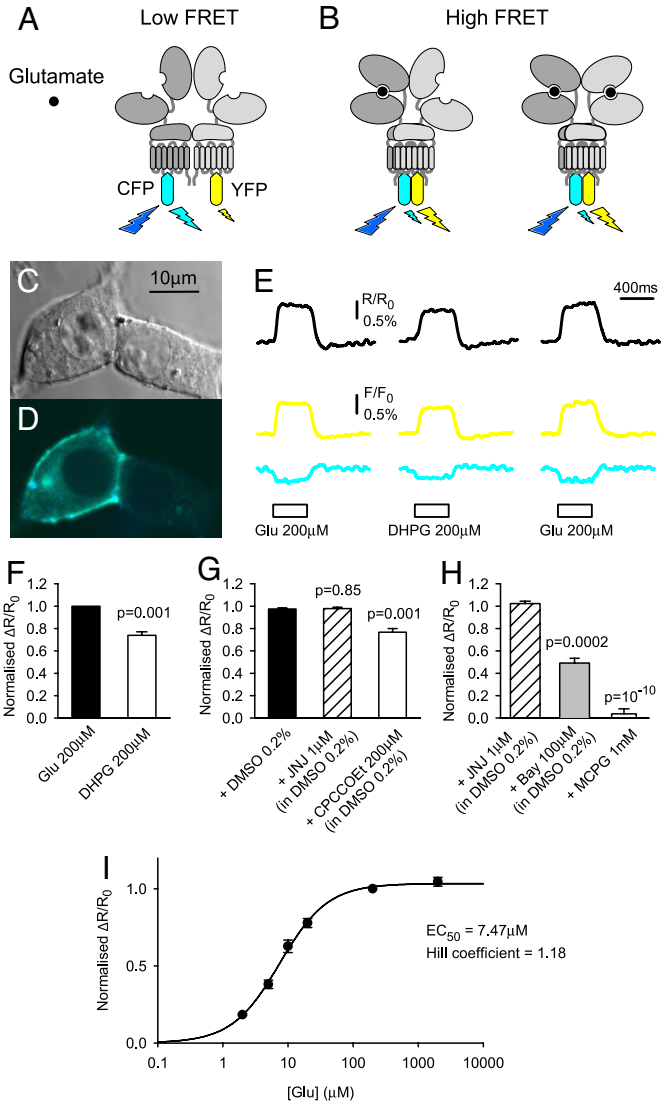

Fig. 1. Detection of mGluR1 activation by FRET. (*A*) Schematic diagram showing CFP or YFP insertion in the second intracellular loop of mGluR1β (mGluR1β-CFP and mGluR1β-YFP, respectively). When co-expressed, the 2 proteins formed dimers as indicated by FRET between CFP and YFP (see Fig. S1). (*B*) Binding of glutamate (black dots) induces a rearrangement of the dimer associated with an increase in FRET (FRET response). According to the proposed structural rearrangement induced by agonist binding, the relative position of the 2 HD should not depend much on whether 1 or 2 VFTM are closed (20, 40). (*C*) Co-expressing PC12 cells visualized in DIC mode. (*D*) Fluorescence image from same cells as in (*C*) when excited at 444 nm. Only highly expressing cells like the one on the left were used for experiments. (*E*) FRET responses to fast application of agonist. Response to 200 μM DHPG bracketed by responses to 200 μM L-glutamate on the same cell. (*F*) Averaged response to 200 μM DHPG normalized to that to 200 μM glutamate. (*G*) Averaged normalized responses to 200 μM glutamate in 0.2% dimethyl sulfoxide (DMSO), in 1 μM JNJ 16259685 + 0.2% DMSO, and in 200 μM CPCCOEt + 0.2% DMSO. For each experiment, the test response was normalized to the response to 200 μM glutamate as in (*E*). (*H*) Averaged normalized responses to 15 μM glutamate in 1 μM JNJ 16259685 (+0.2% DMSO), in 100 μM Bay 36–7620 (+0.2% DMSO) and in 1 mM MCPG. For each experiment, the test response was normalized to the response to 15 μM glutamate as in (*E*). (*I*) Dose-response plot of the FRET response. Application of 2, 5, 10, 20 μM, and 2 mM glutamate were bracketed by application of 200 μM glutamate and normalized to the averaged response to 200 μM glutamate.

Kinetics of Activation and Deactivation. The agonist-induced FRET increase and its recovery upon agonist wash were resolved by single exponentials fits because of the low signal to noise ratio for high

PHARMACOLOGY

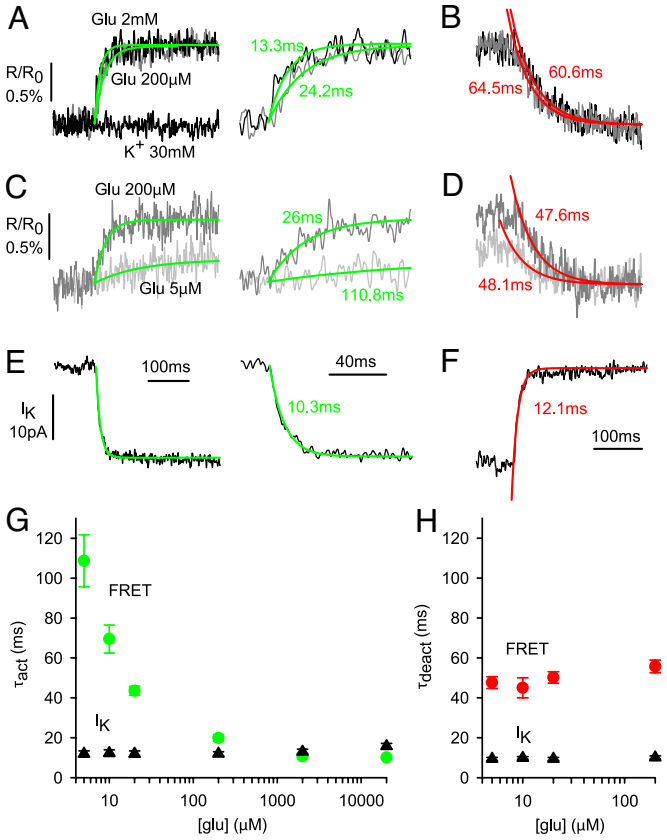

Fig. 2. Activation and deactivation of mGluR1. (*A*) Superimposed FRET responses to 2 mM (black trace) and 200 μM (dark gray) glutamate co-applied with 30 mM K^+, and to 30 mM K^+ alone (black). Note the absence of effect of 30 mM K^+ alone. Right panel shows the responses to glutamate on an expanded time scale. Responses were fitted by single exponentials (green lines) whose time constants are indicated. (*B*) Superimposed FRET responses to wash of 2 mM (black) and 200 μM (dark gray) glutamate. Recoveries were fitted by single exponentials (red lines) whose time constants are indicated. (*C*) Superimposed FRET responses to 200 μM (dark gray) and 5 μM (gray) glutamate co-applied with 30 mM K^+. Right panel shows the responses to glutamate on an expanded time scale. (*D*) Superimposed FRET responses to wash of 200 μM (dark gray) and 5 μM (gray) glutamate. (*E* and *F*) Recorded potassium evoked currents I_K(30 mM K^+) for the experiment illustrated in (*A* and *B*) with same time scale. I_K(30 mM K^+) rise and decay at wash were fitted by single exponentials whose time constant were taken as index for solution exchange at the cell membrane. (*G* and *H*) Averaged activation (*G*) and deactivation (*H*) time constants as a function of glutamate concentration.

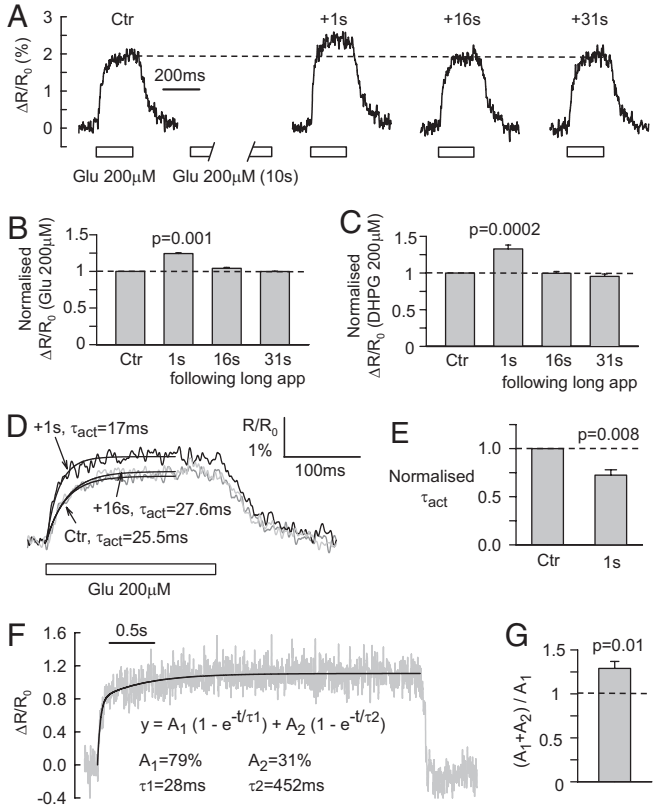

Fig. 3. Sensitization of mGluR1. (*A*) Sensitization produced by 10-s glutamate application. Glutamate (200 μM) was applied for short duration (200 ms) before (ctr) and 1 s, 16 s, and 31 s following a 10-s application. The response measured 1 s following the 10-s application was approximately 25% bigger than the response measured before the 10-s application. (*B*) Averaged normalized glutamate responses obtained from 3 experiments as in (*A*). (*C*) Averaged normalized responses to 200 μM DHPG obtained from 10 experiments as in (*A*). (*D*) FRET response to 200 μM glutamate before (dark gray trace), 1s after (black trace), and 16 s after (gray trace) a 10-s application, on an expanded time scale. The indicated activation time constants were determined by monoexponential fits. (*E*) Averaged change in the activation time constant produced by sensitization. (*F*) Sensitization time course observed for a long (3.2-s) application of 200 μM glutamate. The FRET response to glutamate was fitted by a double exponential whose equation and parameters are shown. (*G*) Sensitization effect measured as the contribution of the second exponential to the FRET response at the end of a long application.

frequency acquisition (Fig. 2*A–D*). The activation time constants could be resolved for glutamate concentrations below 200 μM since they were larger than that of the solution exchange (Fig. 2*E–G*). However the activation time constant for concentrations above 2 mM was not significantly different from the time constant of the solution exchange, saturating at an apparent minimum value of 10.1 ± 0.7 ms (n = 7) for 20 mM glutamate. The deactivation time constant did not depend on the glutamate concentration before wash, and was clearly slower than the solution exchange with a mean value of 51.3 ± 1.9 ms (n = 41; Fig. 2*H*).

Sensitization. We investigated whether long-lasting agonist application could induce desensitization as reported for native GPCRs (27). However, we did not observe desensitization of the FRET response even with glutamate concentration as high as 1 mM and glutamate exposure times up to tens of minutes. As shown in Fig. 3*A* and *B*, when glutamate was applied 1s after a long (10-s) glutamate exposure, the FRET response was potentiated by 24.4 ± 0.9% (P = 0.001). A similar potentiation was observed for longer glutamate exposure (Fig. S4*A*), unpatched cells (Fig. S4*B* and *C*), glutamate exposure in absence of co-applied 30 mM K^+ (n = 3), or exposure to DHPG (Fig. 3*C*), ruling out the possibility that it was caused by side effects of K^+ or glutamate. The FRET response did not desensitize at later times (Fig. S4*B* and *C*). In addition to increasing the amplitude of the FRET response to glutamate, this *sensitization* accelerated the activation rate by 41 + 12% (n = 4; Fig. 3*D* and *E*). For long glutamate applications, the FRET response was best fitted by a double exponential A_1*[1-exp(-t/τ_{a1})]+A_2*[1-exp(-t/τ_{a2})] (Fig. 3*F*) with A_1 = 78.6 ± 4.5%, τ_{a1} = 19.7 ± 3.7 ms, A_2 = 21.4 ± 4.5%, τ_{a2} = 363 ± 54 ms (n = 5; Fig. 3*F*). The sensitization derived from the second exponential fit (Fig. 3*G*) was comparable to the sensitization observed with the preexposure protocol. The accelerated activation of the sensitized receptor (Fig. 3*D* and *E*) along with the independence of the sensitization from the duration of illumination (Fig. 3*A* versus 3*F*) demonstrates that it is mGluR1s and not the fluorescent proteins that are sensitized.

Kinetic Model of mGluR1 Agonist-Induced Rearrangements. Activation of mGluR1 can be "partial" when 1 VFTM only is closed or

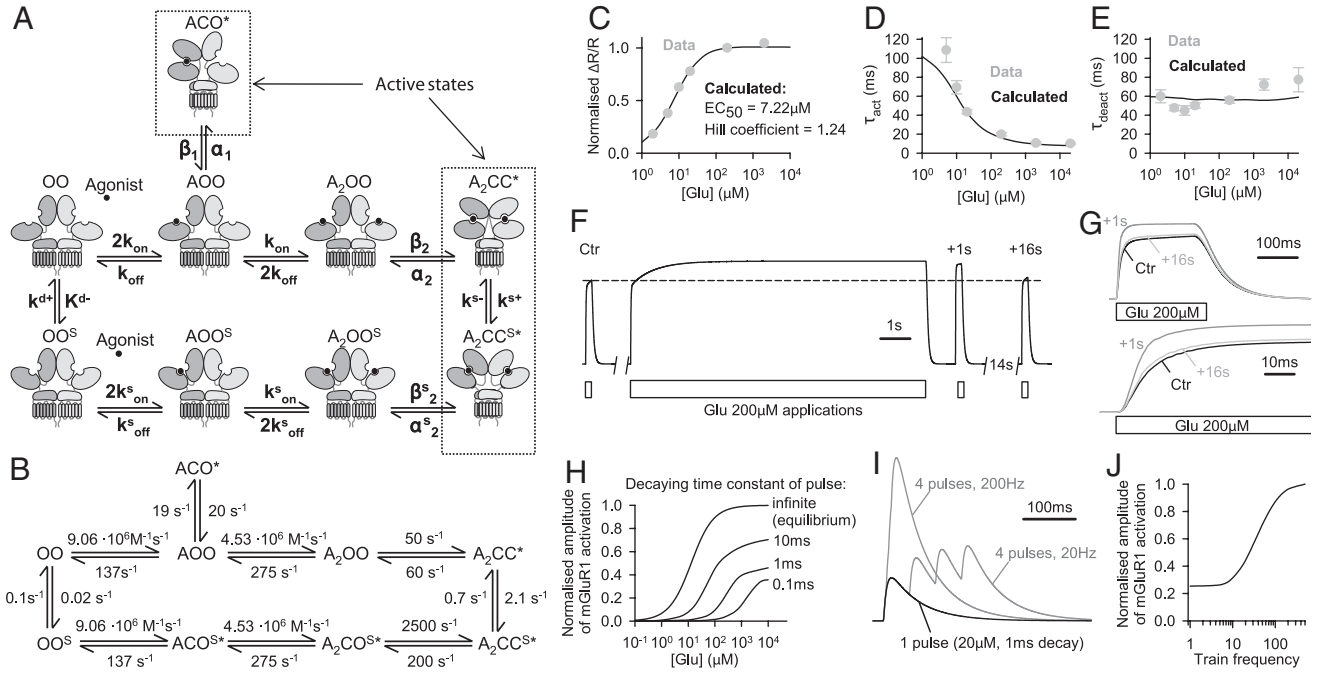

Fig. 4. Modeling of mGluR1 kinetics. (*A*) Kinetic scheme. The sensitized states are shown in the bottom line of the scheme. Following the notation of Pin and coll (40) states are named according to the open (O) or closed (C) conformation of the VFTMs. States are: OO, initial resting state; AOO, resting state bound to 1 agonist; A_2OO, resting state bound to 2 agonists; ACO*, active state bound to 1 agonist with 1 VFTM closed; A_2CC^*, active state bound to 2 agonists with both VFTM closed; A_2CC^{S*}, sensitized active state bound to 2 agonists with both VFTM closed; A_2OO^S, sensitized resting state bound to 2 agonists; AOO^S, sensitized resting state bound to 1 agonist; OO^S, sensitized resting state. We ignored a possible ACO^{S*} state (symmetrical to the ACO* state) because we cannot derive information on the associated rate constants from experimental data. (*B*) Rate constants obtained for the model in (*A*) to fit experimental data. (*C–G*) Simulated mGluR1 activation obtained with rate constants shown in (*B*). The calculated dose-response values (200 ms agonist application) (*C*), activation time constant (*D*) and deactivation time constant (*E*) are shown as continuous black lines and overlapped with the experimental values (filled gray circles). The calculated time course of sensitization during a prolonged application of glutamate (*F*) and the sensitization of the response to short applications (*G*) are in good agreement with the experimental observations (see Fig. 3). (*H*) Calculated dose-response curves at steady state (equilibrium) and for glutamate pulses with exponential decays of 10, 1, or 0.1 ms. (*I*) Calculated activation induced by a 20-μM glutamate pulse with an exponential decay of 1 ms compared with activation induced by trains of 4 identical glutamate pulses (at 20 Hz and 200 Hz). (*J*) Frequency dependency of the amplitude of mGluR1 activation calculated from simulations as in (*I*).

"full" when the 2 VFTMs of the dimeric assembly are closed (28). In accordance with that finding, we initially explored a model with 2 active conformations: 1 closed VFTM and 1 bound agonist (ACO*), 2 closed VFTM and 2 bound agonists (A_2CC^*) (Fig. 4*A*). To account for the sensitization observed during prolonged exposure to glutamate (Fig. 3*F*) we added a third active state (A_2CC^{S*}). The time course of the FRET response to 4 different glutamate concentrations (10, 20, 200, and 2,000 μM) was calculated from the initial guesses for the rates of the model in Fig. 4*A* and the rates were iteratively adjusted to obtain the best fit of the responses. A good reproduction of the observed dose-response curve (Fig. 4*C*), rise time (4*D*) and deactivation time course (4*E*) at all tested concentrations was obtained using the binding and activation rates in the non sensitized part of the model as free parameters (k_{on}, k_{off}, α_1, β_1, α_2, and β_2), assuming equivalent and non-interacting binding sites. The simplest quantitative description of the observed sensitizationof short pulses following long glutamate pulses (Fig. 3 *A–E*) is given by a proportion of the receptors remaining trapped in a "sensitized" conformation from which they can deactivate and eventually lose the agonist molecule, but from which activation is facilitated (second line of states in the model of Fig. 4*A*). We assumed that the binding rates are identical in the non-sensitized and the sensitized states. The forward rate to the sensitized state (k^{s+}) was determined from the slow rising phase of the response to long glutamate applications while the rate for the reversal of this reaction (k^{s-}) was fixed by imposing microscopic reversibility. The rates of entry and exit into the sensitized conformation (k^{d-} and k^{d+}) in the absence of bound agonist were adjusted to match the observed 25% potentiation following prolonged exposure to glutamate (Fig. 4*F*). The sensitized gating rates (β^s_2 and α^s_2) were determined from the fit of the faster activation rate of the sensitizationresponse and its deactivation rate identical to control responses (compare Fig. 4*G* and the traces in Fig. 3*D*).

The rate constants obtained from the fit of our data (Fig. 4*B*) were used to calculate mGluR1 activation induced by short glutamate exposures mimicking transients of synaptically released glutamate. Our simulations showed a steep increase of the EC_{50} under non-steady state conditions when the duration of agonist exposure was shortened. For glutamate transients with decaying time constant of 10, 1, and 0.1 ms, the EC_{50} was 60 μM, 262 μM, and 1.46 mM, respectively (Fig. 4*H*). We also show a frequency dependent summation of mGluR1 activation induced by short agonist exposure (Fig. 4*I* and *J*) that is consistent with the temporal pattern of synaptic activation required to activate native mGluR1 in brain slices (see below).

Discussion

We report here real time kinetics related to conformational changes of a class C GPCR. We chose mGluR1β because mGluR1's role in synaptic transmission has been extensively studied (16–18, 29, 30) and the β subtype is much more efficiently addressed to the plasma membrane than the α subtype, at least in the absence of specific scaffolding proteins (21, 31). The activation rate we report (time course $\leq$ 10 ms) is if the fastest reported so far for a ligand-gated GPCR (6–9). This finding suggests that despite its remote extracellular location, the VFTM [which is homologous to the binding domain of ionotropic glutamate receptors that activate within tens of micro-

seconds (15)] speeds up the overall conformational change induced by agonist binding. The time resolution of our measurements was limited by the speed of the solution exchange at the cell membrane. As a consequence, 10 ms is an upper limit of the actual fastest time course of activation. From the fast activation rate (Fig. 2) and the absence of detectable delay (Fig. S3) we conclude that what delays and slows the electrophysiological responses mediated by mGluR1 (17, 25, 26) is downstream of the agonist-induced rearrangement of mGluR1 dimers.

The insertion of the fluorescent proteins in the second intracellular loop of mGluR1 disrupts the coupling to G proteins (21) (Fig. S5). However, it is unlikely to affect the initial step of mGluR1 activation that we report here, that is, the rearrangement of the transmembrane domains induced by extracellular glutamate binding. Consistently, the EC_{50} we determined for the FRET construct is similar to the EC_{50} of the native mGluR1. Furthermore, for adenosine A_{2A} and α_{2A}-adrenergic receptors, insertion of a smaller tag instead of a fluorescent protein successfully recued G-protein coupling while not affecting the kinetics measured by FRET (8).

It was recently reported that mGluR activation was voltage sensitive (32, 33). We tested this possibility with the hope that depolarization-induced shift of the dose-response would enable kinetic analysis with perfect time resolution. However, we were unable to detect any voltage sensitivity, possibly because it is expressed downstream of the monitored conformational change or impaired by the insertion of the fluorescent protein. The lack of voltage sensitivity would allow the use of our mGluR1 construct as a glutamate sensor: it is efficiently expressed at the cell membrane, the EC_{50} is in the dynamic range of what is expected to be sensed at extrasynaptic location following vesicular release of glutamate, the activation and deactivation rates are fast enough to enable observation of short and repetitive glutamate transients, the lack of desensitization should enable monitoring of long lasting extracellular glutamate transients like the one that may be produced by glutamate spillover. Thus, it would make a good alternative to sensors based on *E. coli* glutamate-binding protein (34).

The value we find for mGluR1 deactivation time course (~50 ms) predicts summation of mGluR1 activation for trains of short glutamate pulses (as during synaptic release) at frequencies above 20 Hz. This was confirmed by our simulations (Fig. 4*J*). Consistently, 20Hz was reported to be the minimum frequency below which synaptic activation fails to evoke mGluR1-mediated EPSCs in acute rat cerebellar slices (35). Until now, the frequency dependence of mGluR1 activation was considered to reflect only accumulating glutamate spillover that overwhelms extracellular glutamate clearing by glutamate transporters (25, 26, 36). The present data indicate that intrinsic kinetic properties of mGluR1 also account for the stimulus frequency-dependence of mGluR1-mediated responses without the need for glutamate transporters to saturate.

Unexpectedly, we found that mGluR1 intrinsic activation does not desensitize but sensitizes. This sensitization is unlikely to be due to a recruitment of mGluR1 to the cell surface because of its relatively fast time course (400 ms) and because our reporter system was devoid of G protein coupling (and hence downstream signal transduction that could activate receptor trafficking to the membrane). To account for the observed sensitization, we propose that the agonist-bound state "relaxes" into a stabilized, sensitized state. As a consequence, activation and deactivation follow a cycle for long agonist exposure. Such a cycle is intriguingly reminiscent of the kinetic schemes for membrane transporters and, more recently, has also been proposed for voltage-activated proteins (37). The amplitude of the observed intrinsic sensitization is small (~25%), and hence, its function may be limited. However, the lack of desensitization is consistent with the previous finding that mGluR1 receptors can operate as efficient detectors of the low but long lasting extracellular [glutamate] transient produced by glutamate spillover (36).

We provide a kinetic scheme for a GPCR. Such a kinetic scheme is especially useful for mGluRs because they are exposed to brief glutamate transients in physiological conditions, due to the timing and the small volumes involved during vesicular release in the CNS. Despite the necessary simplification of the proposed kinetic scheme, it provides insights into kinetic constants. Such knowledge is essential to understand the molecular mechanism of activation of GPCRs, which compose the largest family of mammalian genes and represent the target of nearly half of used drugs (38). It should also help to better understand GPCRs' functions at central synapses where agonists are released for brief durations.

Methods

Construction Design and Cell Transfection. For making the fusion proteins, either Cerulean (Cer) or Citrine (Cit) fluorescent proteins were inserted at position 703 (second intracellular loop) of mGluR1β. A plasmid (TRE-Cer-Cit) was constructed to carry both the coding sequences of mGluR1β-Cer and mGluR1β-Cit fusion proteins each under the control of a separate tet-response element (TRE). PC12 cells (ATCC) were co-transfected with TRE-Cer-Cit and the previously described plasmid pUHD15 (39) that carries a tet-responsive transcription activator (tTA) under a CMV promoter to drive expression of mGluR1β-Cer and mGluR1β-Cit at a fixed stoichiometry. PC12 cells were cultured in high-glucose DMEM (Gibco-Invitrogen) supplemented with 5% FCS and 10% horse serum and plated 1 day before transfections. Transfections were done as transient co-transfections of the pUHD-15 plasmid and the TRE-Cer-Cit plasmid at a weight ratio of 1:3 respectively using Lipofectamine 2000 (Invitrogen) according to the manufacturer's instructions. One day after transfections, the cells were replated on polyD-lysine coated coverslips at lower densities and used for experiments 24–48 h later.

Patch-Clamp Recording, Imaging, and Fast Solution Changes. A coverslip with PC12 cells was placed in a recording chamber mounted on the stage of an inverted microscope (Eclipse TE-2000, Nikon), and voltage-clamp recordings in the whole-cell configuration were performed using an Axopatch 200B amplifier (Molecular Devices). Clampex software (Molecular Devices) was used for data acquisition and for synchronization of voltage command pulses and fluorescence excitation. PC12 cells were superfused with an external solution containing (in mM): NaCl 150, KCl 4, Hepes 5, glucose 5, $MgCl_2$ 1, $CaCl_2$ 2, and the pH adjusted to 7.40 with NaOH. Solution containing agonists contained 124 mM NaCl and 30 mM KCl to enable detection of solution exchange as potassium-induced current in voltage-clamped cells. Cells were whole-cell patch-clamped to −70mV (junction potential taken into account). Patch pipette resistance were approximately 4 MΩ. Normal intracellular (pipette) solution was (in mM): potassium-gluconate 130, NaCl 10, Hepes 20, EGTA 5, $MgCl_2$ 1, MgATP 3, and the pH adjusted to 7.20 with KOH. When testing the voltage sensitivity, K^+ was replaced by Cs^+ for a better clamp of the cell. Patch-clamping did not appear to affect the amplitude of the FRET response measured ($n = 9$). All of the data presented here were obtained from voltage-clamped cells except for Figs. S2, Figs. S4*B* and *C*, and Fig. S5. Fluorescence was induced by light (444 nm) from a computer controlled monochromator (Polychrome V, T.I.L.L. Photonics) through a 50× oil immersion objective. Fluorescence emission was collected through the objective and directed via a first dichroic mirror (465 nm) and a secondary dichroic (505 nm) mirror onto 2 photodiodes (T.I.L.L. Photonics) behind blocking filters (LP 480 nm and LP 515 nm, cyan and yellow channels). Photodiode signals were digitized along with the electrophysiological signals at 10 kHz using hard- and software described above. When fluorescence signals are shown (Fig. 1*E* and Fig. S3) they were corrected for bleaching by dividing the signal by an extrapolated monoexponential fit of the 500-ms baseline preceding solution exchange. FRET responses were quantified by dividing the fluorescence signal measured in the yellow channel by the fluorescence measured in the cyan channel and expressed as changes in this ratio normalized to baseline ($\Delta R/R_0$). No correction was made for CFP fluorescence detected in the yellow channel or constant offsets; reported $\Delta R/R_0$ are therefore smaller than those that could be obtained with additional corrections and use of narrow band pass filters. Fast solution exchange was achieved using a HSSE-2/3 (Ala Scientific Instruments). Solution exchange inevitably produced small movement artifacts that could be detected as (1) cyan and yellow fluorescence changes in the same direction, (2) fluorescence changes evoked by K^+ (30 mM) application (alone). Data were analyzed only when movement artifacts were below our detection limit and hence did not affect our analysis. Data are shown as means ± SEM. *P* values were obtained from 2-tailed *t*-tests.

Determination of the Kinetic Rates of Activation of mGluR1. Rate constants were determined with ChanneLab software (Synaptosoft Inc.), which uses a Simplex algorithm to find the rate constants that minimize the sum of squared differences between data points and the trace calculated at each iteration. The concentration profile was determined from the time course of the K^+ induced current in the patched cell, appropriately scaled to match each concentration. Since the signal to noise ratio, especially at the lowest concentrations, is too low to allow direct fitting of the rates to the FRET signal, individual traces at each concentration were first fitted with rising and decaying exponentials. Given the small coefficient of variation of the mean activation and deactivation time constants (5–12%), a single model trace was generated from the average time constants for each cell at a given concentration and these traces were used for fitting the kinetic rates.

The use of experimental responses to 3 glutamate concentrations (10, 20, and 200 μM) provided a satisfactory global fit. However, by including the response to 2 mM glutamate, we obtained a better global fit and essential information on β_2, since in the presence of high glutamate, binding is not the limiting factor in determining the rise time of the response.

ACKNOWLEDGMENTS. We thank Yuka Iwamoto for help with cell culture and transfection and Jennifer Yokoyama and Christoph Schwarzer for preparation of mGluR1β-Cer and mGluR1β-Cit and TRE-Cer-Cit plasmids, respectively, and David Colquhoun, David Attwell, Trevor Smart, and Amélie Perron for comments on the manuscript. This work was supported by a Medical Research Council Career Development Award (to P.M.), a Royal Society travel grant (P.M.), and RIKEN intramural grants (to T.K.). M.B. is a Royal Society University Research Fellow.

1. Charpak S, Gahwiler BH, Do KQ, Knopfel T (1990) Potassium conductances in hippocampal neurons blocked by excitatory amino-acid transmitters. *Nature* 347:765–767.
2. Lujan R, Roberts JD, Shigemoto R, Ohishi H, Somogyi P (1997) Differential plasma membrane distribution of metabotropic glutamate receptors mGluR1 alpha, mGluR2, and mGluR5, relative to neurotransmitter release sites. *J Chem Neuroanat* 13:219–241.
3. Conn PJ, Pin JP (1997) Pharmacology and functions of metabotropic glutamate receptors. *Annu Rev Pharmacol Toxicol* 37:205–237.
4. Bergles DE, Jahr CE (1997) Synaptic activation of glutamate transporters in hippocampal astrocytes. *Neuron* 19:1297–1308.
5. Clark BA, Barbour B (1997) Currents evoked in Bergmann glial cells by parallel fibre stimulation in rat cerebellar slices *J. Physiol* 502:335–350.
6. Lohse MJ, et al. (2008) Kinetics of G-protein-coupled receptor signals in intact cells. *Br J Pharmacol* 153:S125–S132.
7. Vilardaga JP, Bunemann M, Krasel C, Castro M, Lohse MJ (2003) Measurement of the millisecond activation switch of G protein-coupled receptors in living cells. *Nat Biotechnol* 21:807–812.
8. Hoffmann C, et al. (2005) A FlAsH-based FRET approach to determine G protein-coupled receptor activation in living cells. *Nat Methods* 2:171–176.
9. Rochais F, et al. (2007) Real-time optical recording of beta1-adrenergic receptor activation reveals supersensitivity of the Arg389 variant to carvedilol. *J Clin Invest* 117:229–235.
10. Makino CL, Wen XH, Lem J (2003) Piecing together the timetable for visual transduction with transgenic animals. *Curr Opin Neurobiol* 13:404–412.
11. Colquhoun D, Sakmann B (1985) Fast events in single-channel currents activated by acetylcholine and its analogues at the frog muscle end-plate. *J Physiol* 369:501–557.
12. Pin JP, et al. (2004) The activation mechanism of class-C G-protein coupled receptors. *Biol Cell* 96:335–342.
13. Kniazeff J, et al. (2004) Locking the dimeric GABA(B) G-protein-coupled receptor in its active state. *J Neurosci* 24:370–377.
14. Kunishima N, et al. (2000) Structural basis of glutamate recognition by a dimeric metabotropic glutamate receptor. *Nature* 407:971–977.
15. Robert A, Howe JR (2003) How AMPA receptor desensitization depends on receptor occupancy. *J Neurosci* 23:847–858.
16. Kano M, Hashimoto K, Tabata T (2008) Type-1 metabotropic glutamate receptor in cerebellar Purkinje cells: A key molecule responsible for long-term depression, endocannabinoid signalling, and synapse elimination. *Philos Trans R Soc Lond B Biol Sci* 363:2173–2186.
17. Batchelor AM, Garthwaite J (1997) Frequency detection and temporally dispersed synaptic signal association through a metabotropic glutamate receptor pathway. *Nature* 385:74–77.
18. Ichise T, et al. (2000) mGluR1 in cerebellar Purkinje cells essential for long-term depression, synapse elimination, and motor coordination. *Science* 288:1832–1835.
19. Romano C, Yang WL, O'Malley KL (1996) Metabotropic glutamate receptor 5 is a disulfide-linked dimer. *J Biol Chem* 271:28612–28616.
20. Muto T, Tsuchiya D, Morikawa K, Jingami H (2007) Structures of the extracellular regions of the group II/III metabotropic glutamate receptors. *Proc Natl Acad Sci USA* 104:3759–3764.
21. Tateyama M, Abe H, Nakata H, Saito O, Kubo Y (2004) Ligand-induced rearrangement of the dimeric metabotropic glutamate receptor 1alpha *Nat Struct Mol. Biol* 11:637–642.
22. Tateyama M, Kubo Y (2006) Dual signaling is differentially activated by different active states of the metabotropic glutamate receptor 1alpha. *Proc Natl Acad Sci USA* 103:1124–1128.
23. Wisniewski K, Car H (2002) (S)-3,5-DHPG: A review. *CNS Drug Rev* 8:101–116.
24. Carroll FY, et al. (2001) BAY36–7620: A potent non-competitive mGlu1 receptor antagonist with inverse agonist activity. *Mol Pharmacol* 59:965–973.
25. Brasnjo G, Otis TS (2001) Neuronal glutamate transporters control activation of postsynaptic metabotropic glutamate receptors and influence cerebellar long-term depression. *Neuron* 31:607–616.
26. Reichelt W, Knopfel T (2002) Glutamate uptake controls expression of a slow postsynaptic current mediated by mGluRs in cerebellar Purkinje cells. *J Neurophysiol* 87:1974–1980.
27. Kelly E, Bailey CP, Henderson G (2008) Agonist-selective mechanisms of GPCR desensitization. *Br J Pharmacol* 153 Suppl 1:S379–S388.
28. Kniazeff J, et al. (2004) Closed state of both binding domains of homodimeric mGlu receptors is required for full activity. *Nat Struct* Mol. *Biol* 11:706–713.
29. Conquet F, et al. (1994) Motor deficit and impairment of synaptic plasticity in mice lacking mGluR1. *Nature* 372:237–243.
30. Takechi H, Eilers J, Konnerth A (1998) A new class of synaptic response involving calcium release in dendritic spines. *Nature* 396:757–760.
31. Kumpost J, et al. (2008) Surface expression of metabotropic glutamate receptor variants mGluR1a and mGluR1b in transfected HEK293 cells. *Neuropharmacology* 55:409–418.
32. Ben-Chaim Y, et al. (2006) Movement of 'gating charge' is coupled to ligand binding in a G-protein-coupled receptor. *Nature* 444:106–109.
33. Ohana L, Barchad O, Parnas I, Parnas H (2006) The metabotropic glutamate G-protein-coupled receptors mGluR3 and mGluR1a are voltage-sensitive. *J Biol Chem* 281:24204–24215.
34. Hires SA, Zhu Y, Tsien RY (2008) Optical measurement of synaptic glutamate spillover and reuptake by linker optimized glutamate-sensitive fluorescent reporters. *Proc Natl Acad Sci USA* 105:4411–4416.
35. Tempia F, Miniaci MC, Anchisi D, Strata P (1998) Postsynaptic current mediated by metabotropic glutamate receptors in cerebellar Purkinje cells. *J Neurophysiol* 80:520–528.
36. Marcaggi P, Attwell D (2005) Endocannabinoid signaling depends on the spatial pattern of synapse activation. *Nat Neurosci* 8:776–781.
37. Villalba-Galea CA, Sandtner W, Starace DM, Bezanilla F (2008) S4-based voltage sensors have three major conformations. *Proc Natl Acad Sci USA* 105:17600–17607.
38. Howard AD, et al. (2001) Orphan G-protein-coupled receptors and natural ligand discovery. *Trends Pharmacol Sci* 22:132–140.
39. Gossen M, Bujard H (1992) Tight control of gene expression in mammalian cells by tetracycline-responsive promoters. *Proc Natl Acad Sci USA* 89:5547–5551.
40. Pin JP, Galvez T, Prezeau L (2003) Evolution, structure, and activation mechanism of family 3/C G-protein-coupled receptors. *Pharmacol Ther* 98:325–354.